The active site dynamics of 4-chlorobenzoyl-CoA dehalogenase

Edmond Y. Lau and Thomas C. Bruice*

Department of Chemistry and Biochemistry, University of California, Santa Barbara, CA 93106

Contributed by Thomas C. Bruice, June 5, 2001

A molecular dynamics study was performed to compare the differences in the active-site dynamics of the wild-type and W137F mutant enzymes of 4-chlorobenzoyl-CoA dehalogenase. Only in the wild-type simulation are conformations formed between the catalytic Asp-145 and 4-chlorobenzoyl-CoA, which resemble the *ab initio* calculated gas-phase transition-state geometry. In the W137F simulation, the hydrogen bond formed between His-90 and Asp-145 persisted throughout the simulation, causing the carboxylate of Asp-145 to be distant from the benzoyl ring of 4-chlorobenzoyl-CoA. In both simulations, water molecules were able to diffuse into the active site of the enzymes. The trajectories provide insight into the routes that water may use to get into position for the hydrolysis portion of the dehalogenation reaction. In both simulations, the water molecule entering the active site forms a hydrogen bond with Asp-145.

Enzymes are able to catalyze a wide variety of reactions. Through evolution, bacteria can adapt to available sources of nutrient. Halogenated solvents are industrial pollutants that are difficult to degrade and are now commonly found in the environment. Certain bacteria have developed the ability to use halogenated solvents as their primary carbon source. Bacterial enzymes such as haloalkane dehalogenase and haloacid dehalogenase can cleave carbon-halogen bonds. Interestingly, these enzymes use different mechanisms to catalyze the dehalogenation reaction (1–3). There has been a great deal of interest in using dehalogenase enzymes for bioremediation (4). *Pseudomonas* sp. strain CBS-3 carries out the conversion of 4-chlorobenzoate to 4-hydroxybenzoate. Three enzymes within the bacterium carry out the conversion reaction with 4-chlorobenzoyl-CoA (4-CBA-CoA) dehalogenase, performing the difficult task of cleaving the carbon-halogen bond of 4-CBA-CoA to form 4-hydroxybenzoyl-CoA (4-HBA-CoA; refs. 5–7). The crystal structure of this enzyme with the bound product has been solved at high resolution (1.8 Å) and shows that the crystallized complex exists as a trimer (8). The 4-HBA-CoA is bound in the active site primarily formed from two subunits. The crystal structure shows that much of the polypeptide chain (78%) is involved in secondary structure. Each subunit consists of 269 residues that form 8 α-helices and 10 strands of β-sheet.

The dehalogenation reaction occurs by means of an S_NAr mechanism initiated by nucleophilic attack at the C4 of the benzoyl group (BC4) of 4-CBA-CoA by the carboxylate of Asp-145 to form a Meisenheimer intermediate (Scheme 1; refs. 1, 2, and 9). The chloride is displaced from the Meisenheimer intermediate because of rearomatization of the benzoyl group to form an enzyme–ester. This enzyme–ester subsequently is hydrolyzed to form 4-HBA-CoA by an activated water molecule. The general base in the hydrolysis reaction is His-90, based on mutation experiments and its proximity to Asp-145 (10). Much of the active site is composed of hydrophobic residues, except for the catalytic Asp-145 and His-90. The crystal structure shows the benzoyl group of 4-HBA-CoA is surrounded by the side chains of Phe-64, Phe-82, Trp-89, and Trp-137 (Fig. 1). The aromatic groups around the benzoyl ring likely assist in the polarization of the π-electrons in the benzoyl ring during the reaction (11, 12). Mutation studies of this enzyme by Dunaway-Mariano and coworkers (13) have shown that Trp-137, which forms a hydrogen bond with the catalytic Asp-145, has a significant effect on the formation of the Meisenheimer intermediate. Although the overall catalytic constant, k_{cat}, for the conversion of 4-CBA-CoA to 4-HBA-CoA is reduced only ≈60-fold when Trp-137 is mutated into a phenylalanine (13), the rate of forming the Meisenheimer intermediate is reduced 20,000-fold for this mutant (D. Dunaway-Mariano, personal communication). Comparison of the crystal structures of the wild-type (WT) and W137F mutant enzymes shows that the side chain of Asp-145 has reoriented in the W137F enzyme to be pointing almost 180° from the direction in the WT. The carboxylate of Asp-145 in W137F forms a hydrogen bond to His-90, the general base in the hydrolysis reaction. In this geometry, the carboxylate is too far from BC4 of 4-CBA-CoA to form the Meisenheimer intermediate. Only with a large scale change in the Asp-145 side chain can a reactive conformation be formed in this mutant enzyme.

A molecular dynamics study of the active site of 4-CBA-CoA dehalogenase has been performed for the WT and W137F enzymes. Both simulations were performed for a total of 2.4 ns by using stochastic boundary molecular dynamics techniques centered on the active site of subunit A of the enzyme. Both simulations contained much of subunit A and portions of subunits B and C. The simulations show that only the WT enzyme is able to form reactive conformers during the trajectory. Within the time scale of these simulations, Asp-145 in the W137F simulation does not break its hydrogen bond with His-90. Additionally, both simulations show that a water molecule is able to diffuse into the active site and hydrogen-bonds to Asp-145. The three active sites of this trimeric enzyme do not contain water in the crystal structure.

Methods

Stochastic boundary molecular dynamics (14) was performed on the active site of the WT (Protein Data Bank ID code 1NZY; ref. 8) and W137F mutant 4-CBA-CoA dehalogenase (provided by H. Holden, Univ. of Wisconsin, Madison, WI). The program CHARMM was used for the molecular dynamics simulations (15). A sphere of 35-Å radius centered on BC4 of 4-HBA-CoA was cut out of subunit A in both the WT and W137F enzyme. Crystallographic water molecules greater than 30 Å from Asp-145 were deleted. The active sites were solvated in a sphere of 30-Å radius of TIP3P water, using BC4 of 4-HBA-CoA as the origin (16). If any oxygen of a water molecule was within 2.8 Å of a heavy atom of the enzyme or a crystallographic water, that water molecule was deleted. The WT system contained 11,900 atoms, and the W137F system

Abbreviations: 4-CBA-CoA, 4-chlorobenzoyl-CoA; 4-HBA-CoA, 4-hydroxybenzoyl-CoA; WT, wild-type 4-CBA-CoA dehalogenase; W137F, mutant 4-CBA-CoA dehalogenase containing phenylalanine at residue 137; BC4, C4 of the benzoyl group; NAC, near attack conformer; BO, carbonyl oxygen.

*To whom reprint requests should be addressed. E-mail: tcbruice@bioorganic.ucsb.edu.

The publication costs of this article were defrayed in part by page charge payment. This article must therefore be hereby marked "*advertisement*" in accordance with 18 U.S.C. §1734 solely to indicate this fact.

BIOCHEMISTRY

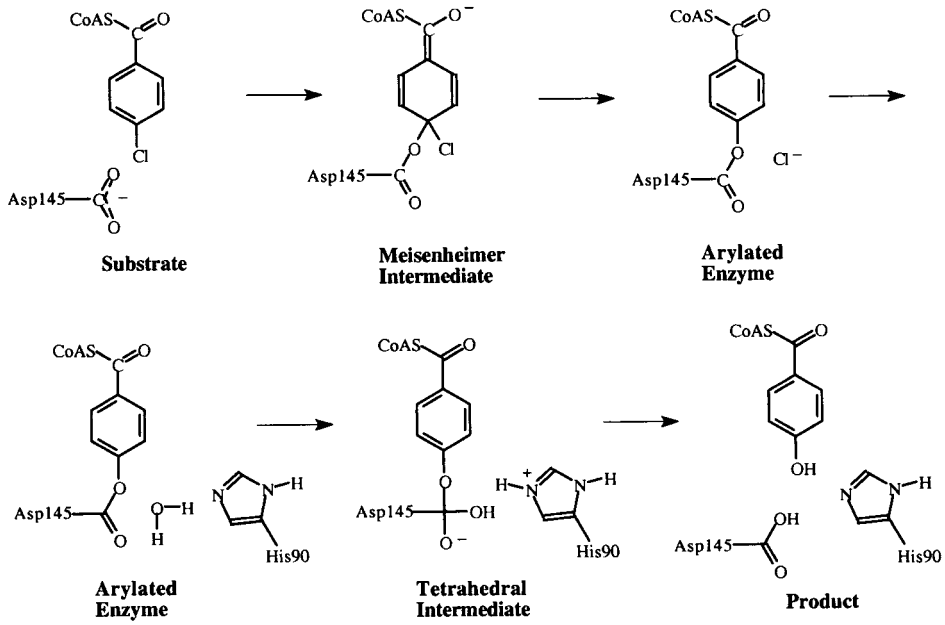

Scheme 1.

contained 11,939 atoms. Protein atoms greater than 30 Å from the origin were fixed in position. The catalytic His-90 was modeled as a neutral residue in both simulations but, based on the crystal structures, His-90 in the WT enzyme has a proton on the ND1 atom of the imidazole, and His-90 in the W137F mutant has the proton on the NE2 atom; both were modeled accordingly. In addition, His-7 and His-23 in subunit A and His-208, His-244, and His-256 in subunit B were modeled as protonated residues. These histidines are distant from the active site. The overall charge of both systems is −1. The crystal structure of 4-CBA-CoA dehalogenase contains the product 4-HBA-CoA in the active site. In both simulations, the 4-HBA-CoA was replaced with 4-CBA-CoA. 4-chlorobenzoyl-CoA was built from the adenine-residue topology file included with the software program QUANTA from MSI (Molecular Simulations, Waltham, MA). Charges for the benzoyl and pantothenate groups in 4-CBA-CoA were obtained from HF/6–31+G(d) calculations with the ChelpG charge-fitting procedure (17). The *ab initio* calculations and the charge-fitting were performed with GAUSSIAN 98 (18). All other atoms in 4-CBA-CoA used the MSI charges. MSI parameters for the force constants and van der Waals terms were used for these simulations. The same protocols for energy minimization and dynamics were used for both simulations. The two initial structures were energy-minimized by using a combination of steepest descents and adopted basis Newton-Rapheson methods (15). A buffer region of 2 Å was used between 28 and 30 Å. The system was coupled to a heat bath using a frictional coefficient of 250 ps^{-1} on heavy-protein atoms; the oxygens of water molecules had a frictional coefficient of 62 ps^{-1}. Constraining forces for heavy protein atoms in the buffer region were constructed from their average Debye–Waller factors (14). All water molecules were constrained to remain within 30 Å of the origin by a radial potential (19). The Langevin equation was used to integrate the equations of motions (20). A time step of 2 fs was used, and the nonbonded list was updated every 20 time steps. The nonbonded interactions were cut off at 12 Å by using a shifting function on the electrostatic energy; a switching function from 10 to 11 Å was used for the van der Waals potential. The SHAKE algorithm was used to constrain bonds containing hydrogens to their equilibrium length (21). The system was initially coupled to a heat bath at 100 K for 300 ps. After this period, the system was coupled to a heat bath at 200 K for 300 ps then coupled to a heat bath at 300 K. The heating and equilibration were performed for a total of 1 ns. Production dynamics were performed for 1.4 ns. The coordinates were saved every 100 time steps. Both simulations were performed for this period.

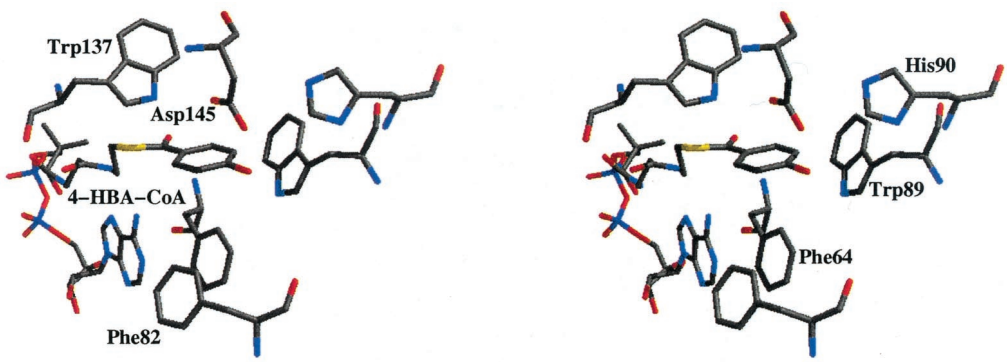

Fig. 1. Stereo picture of the active site of 4-CBA-CoA dehalogenase containing 4-HBA-CoA. This picture was created from the crystal structure 1NZY.

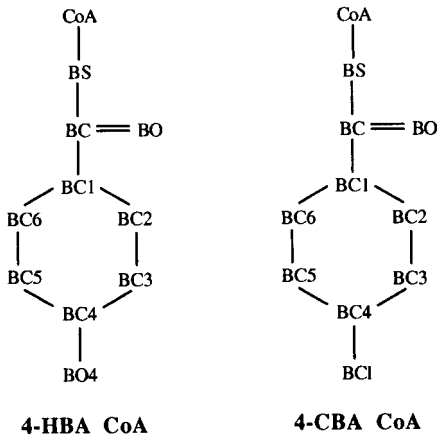

Fig. 2. Labeling used to describe the atoms in the benzoyl group of 4-CBA-CoA and 4-HBA-CoA.

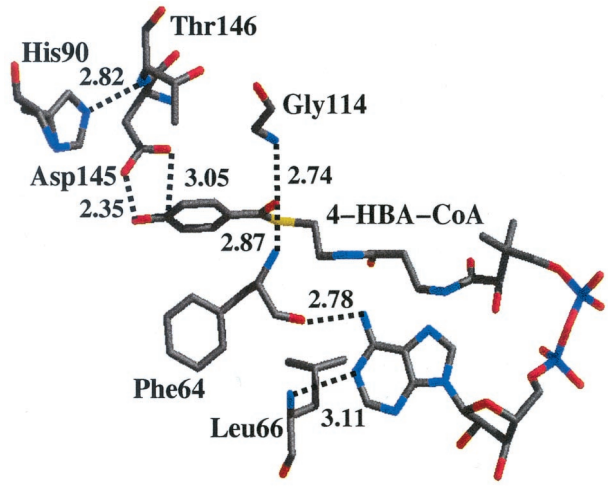

Fig. 3. Picture of important hydrogen bonds in the active site of 4-CBA-CoA dehalogenase. The values in the pictures are given in Å. The picture was made from the crystal structure 1NZY.

Results and Discussion

In the crystal structure, 4-HBA-CoA is folded over in the active site of 4-CBA-CoA dehalogenase such that the benzoyl group is in the same proximity to the adenine (see Fig. 1). The benzoyl group of 4-HBA-CoA is bound in a primarily hydrophobic environment. There are only two residues within 8 Å of the BC4 that are highly polar (Asp-145 and His-90), but there are eight nonpolar residues (Phe-64, Phe-82, Ala-85, Trp-89, Gly-113, Trp-137, and Ile-142 from subunit A and Val-236 from subunit C). It has been shown experimentally that mutation of Trp-137 to a phenylalanine causes a 20,000-fold reduction in the rate of formation of the Meisenheimer intermediate (D. Dunaway-Mariano, personal communication). This residue does not directly participate in the chemical step in the reaction, but from the crystal structure this tryptophan positions the catalytic Asp-145 (nucleophile) by the BC4 of 4-HBA-CoA (see Fig. 2 for benzoyl numbering). Mutation of Trp-137 does not affect binding of the substrate (10). The carboxylate geometry of Asp-145 is stabilized by two hydrogen bonds (Trp-137 NE1 to Asp-145 OD1 and 4-HBA-CoA BO4 to Asp-145 OD2). The precise positioning of Asp-145 is critical in the dehalogenation reaction. In addition to the W137F mutant's reduced ability to form the Meisenheimer intermediate, the mutant D145E dehalogenase has a k_{cat} that is 600 times lower than that of the WT enzyme (22). The simple addition of an extra carbon to the nucleophilic side chain has a significant effect on catalysis.

The interactions between 4-CBA-CoA and the enzyme are stable for the duration of the dynamics trajectories. In the crystal structure, hydrogen bonds are formed between the backbone amides of Phe-64 and Gly-114 to the carbonyl oxygen (BO) of the 4-HBA-CoA (Fig. 3). These hydrogen bonds between the carbonyl oxygen and the backbone amides stabilize the increased charge in the benzoyl ring upon forming the transition state (12). In the WT simulation, the distance of Phe-64 N to BO of 4-CBA CoA was 3.16 ± 0.22 Å and the distance of Gly-114 N to BO of 4-CBA-CoA was 2.95 ± 0.19 Å. In the W137F mutant simulation, the distance of Phe-64 N to BO of 4-CBA-CoA was 3.05 ± 0.19 Å and the distance of Gly-114 N to BO of 4-CBA-CoA was 2.97 ± 0.17 Å. In the crystal structure, the conformation of the adenine of 4-HBA-CoA is stabilized by hydrogen bonds between the backbone N of Leu-66 and the adenine AN1 of 4-HBA-CoA and the backbone O of Phe-64 to the adenine AN6 of 4-HBA-CoA. These hydrogen bonds are persistent throughout the WT and W137F simulations (see Table 1). The orientation of the imidazole of His-90 (general base) is stabilized by a hydrogen bond between ND1 of His-90 and a backbone carbonyl O of Ala-86 in the WT simulation. The average distance for this interaction (N···O) was 2.84 ± 0.13 Å. This hydrogen bond is not present in the W137F simulation, and the imidazole ring is rotated almost 90° from its configuration in the WT simulation. The dihedral angle formed by CA–CB–CG–CD2 in His-90 was −91.0° ± 11.4° and −8.0° ± 14.0° in the WT and W137F simulations, respectively.

The conformation for Asp-145 in the crystal structure should not be expected in the Michaelis complex with 4-CBA-CoA. The hydroxyl group on the benzoyl ring of 4-HBA-CoA is not present in the substrate 4-CBA-CoA, eliminating the stabilizing hydrogen bond between BO4 and Asp-145 OD2. The OD2 of Asp-145 moved away from the benzoyl ring during the WT dynamics simulation and formed a hydrogen bond with the backbone amide of Thr-146 that was stable for the remainder of the simulation (2.87 ± 0.14 Å, N···O distance). Because of this hydrogen bond, the angles formed between OD2 of Asp-145 and the atoms in the 4-CBA-CoA benzoyl group are not similar to the calculated transition-state structure of Zheng and Bruice for this reaction (23). Ground-state structures resembling the transition-state structure are known as near attack conformers (NACs; refs. 24, 25). A NAC was defined for structures in the dehalogenase as follows: the distance between one of the carboxylate

Table 1. Average values obtained from the simulations

Measurement	WT	W137F
Distance, Å		
CBA BC4–Asp145 OD1	3.26 ± 0.21	5.40 ± 0.58
CBA BC4–Asp145 OD2	3.67 ± 0.29	4.98 ± 0.77
CBA BO–Phe64 N	3.16 ± 0.22	3.05 ± 0.19
CBA BO–Gly114 N	2.95 ± 0.19	2.97 ± 0.17
His-90 ND1–Ala86 O	2.84 ± 0.13	3.56 ± 0.29
His-90 NE2–Asp145 OD1	5.86 ± 0.43	3.00 ± 0.30
Angle, °		
Asp-145 OD1–CBA BC4–CBA BC3	96.5 ± 11.7	112.2 ± 14.7
Asp-145 OD1–CBA BC4–CBA BC5	82.1 ± 10.4	107.9 ± 16.8
Asp-145 OD2–CBA BC4–CBA BC3	131.4 ± 11.5	122.3 ± 15.0
Asp-145 OD2–CBA BC4–CBA BC5	72.5 ± 9.7	95.6 ± 17.6
Dihedral, °		
His-90 CA–CB–CG–CD2	−8.0 ± 14.0	−91.0 ± 11.4

CBA is used as the abbreviation for 4-CBA-CoA.

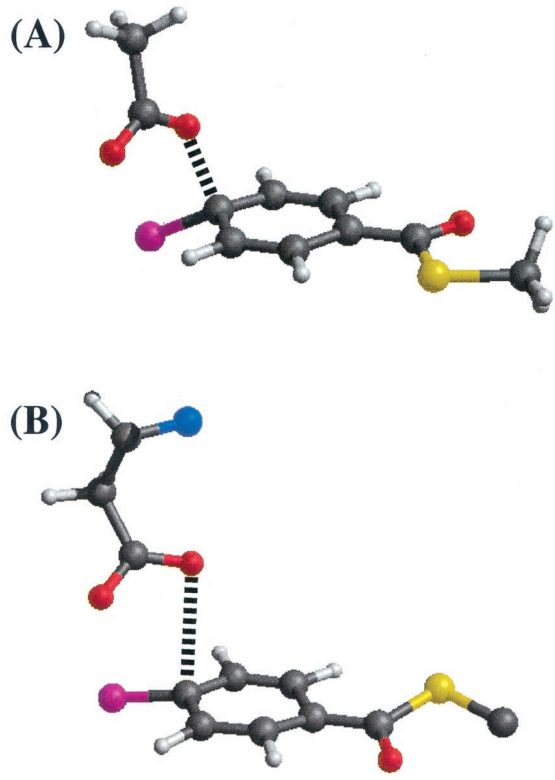

Fig. 4. (*A*) The *ab initio* transition state calculated by Zheng and Bruice (23) for acetate attack on a thioester of 4-chlorobenzoic acid. (*B*) A NAC between Asp-145 and 4-CBA-CoA from dynamics. The dashed line shows the closest carboxylate oxygen to the C4 of the substrate.

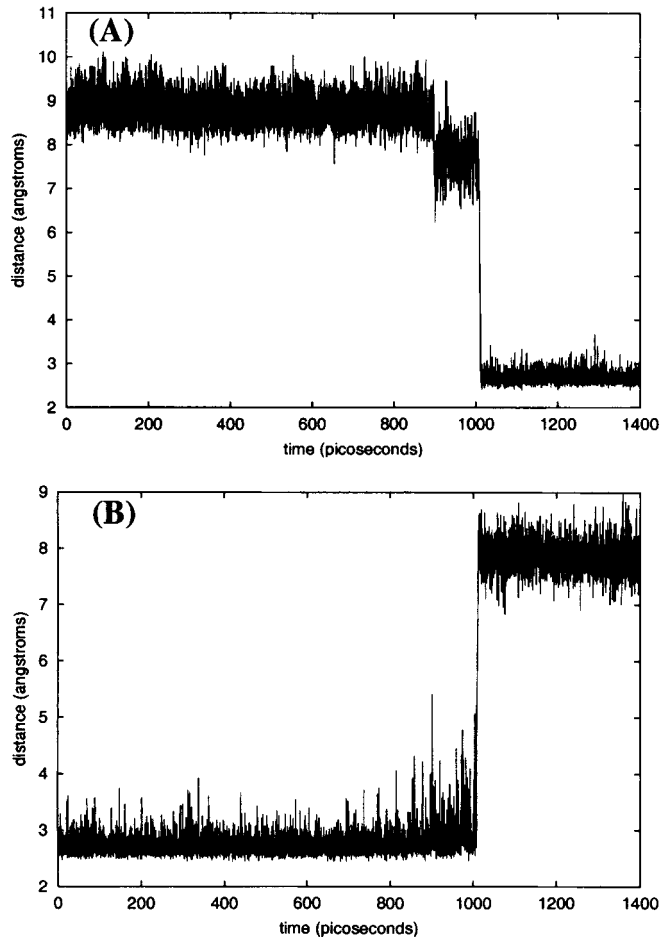

Fig. 5. (*A*) The distance between Asn-144 OD1 and the oxygen of the water molecule entering the active site from the WT simulation during production dynamics. (*B*) The distance between Asp-145 OD1 and the oxygen of the water molecule entering the active site during production dynamics.

oxygens of Asp-145 to BC4 of 4-CBA-CoA was 3.2 Å or less, and the angles formed by the carboxylate oxygen and BC4-BC3 of 4-CBA-CoA and oxygen and BC4-BC5 of 4-CBA-CoA were between 90° and 120° for both angles. The angular distribution allows an ≈15° deviation from the angles obtained from the HF/6–31+G(d) transition-state structure of Zheng and Bruice (23). The distance-dependence of the O···C separation for a NAC has been used successfully for predicting the rate enhancement in strain-free cyclization reactions of dicarboxylic acids to form anhydrides (26). The number of NACs sampled by the dicarboxylic acids was shown to correlate with the relative rate enhancement for anhydride formation.

The OD2 of Asp-145 is in close proximity to BC4 of 4-CBA-CoA (3.67 ± 0.29 Å), but the average angles are 131.4° ± 11.5° for OD2–BC4–BC3 and 72.5° ± 9.7° for OD2–BC4–BC5. Only OD1 of Asp-145 is in position to form a reactive conformer during production dynamics in the WT enzyme. Only the WT enzyme was able to form conformations that are catalytically productive (NACs) within the duration of the simulations. In the WT simulation, NACs are present in 4.6% (646/14,000) of the collected coordinates of the simulation. Interestingly, the average conformation of Asp-145 to the 4-CBA-CoA is almost a NAC. The average OD2 of Asp-145 to BC4 of 4-CBA-CoA distance is 3.26 ± 0.21 Å, and the angles formed by OD2 of Asp-145 with the BC4 and BC3 of 4-CBA-CoA and BC4 and BC5 were 96.5° ± 11.7° and 82.1° ± 10.4°, respectively. Fig. 4 shows the similarity between the *ab initio* transition-state structure calculated by Zheng and Bruice and a NAC structure from the WT simulation. Formation of the OD2 of Asp-145 to backbone N of Thr-146 hydrogen bond displaces His-90 from its position in the crystal structure. The NE2 of His-90 likely is hydrogen-bonded to this backbone amide in the crystal structure because the N···N distance is 2.82 Å. The imidazole ring backs away from Asp-145 during dynamics, increasing the separation between these two residues. The increased separation between these two residues may be favorable in accommodating a water molecule.

In the mutant enzyme, the hydrogen bond between the Asp-145 OD1 and His-90 NE2 persists throughout the simulation. This hydrogen bond prevents the carboxylate of the catalytic Asp-145 from forming structures with the 4-CBA-CoA that are similar to the transition state. Although OD2 of Asp-145 is closer to BC4, the O···C distance does not come within 3.2 Å (Table 1). No NACs were formed in the mutant simulation during the trajectory. Experimentally, Dunaway-Mariano and coworkers (13) have shown two absorption bands are prominent when the WT enzyme binds 4-HBA-CoA. The band corresponding to a λ_{max} at 373 nm has Asp-145 near the 4-position of the benzoyl. A smaller band at 330 nm corresponds to a conformational change in Asp-145 that is not positioned for reacting. In the W137F mutant enzyme, there is a slow interconversion from the 373-nm band to the 330-nm band. 4-HBA-CoA in solution has a λ_{max} at 292 nm and a shoulder near 335 nm. In the mutant D145E, only the 330-nm band is present, and the enzyme has reduced activity (22). The pair of bands in the WT enzyme leads to the conclusion that

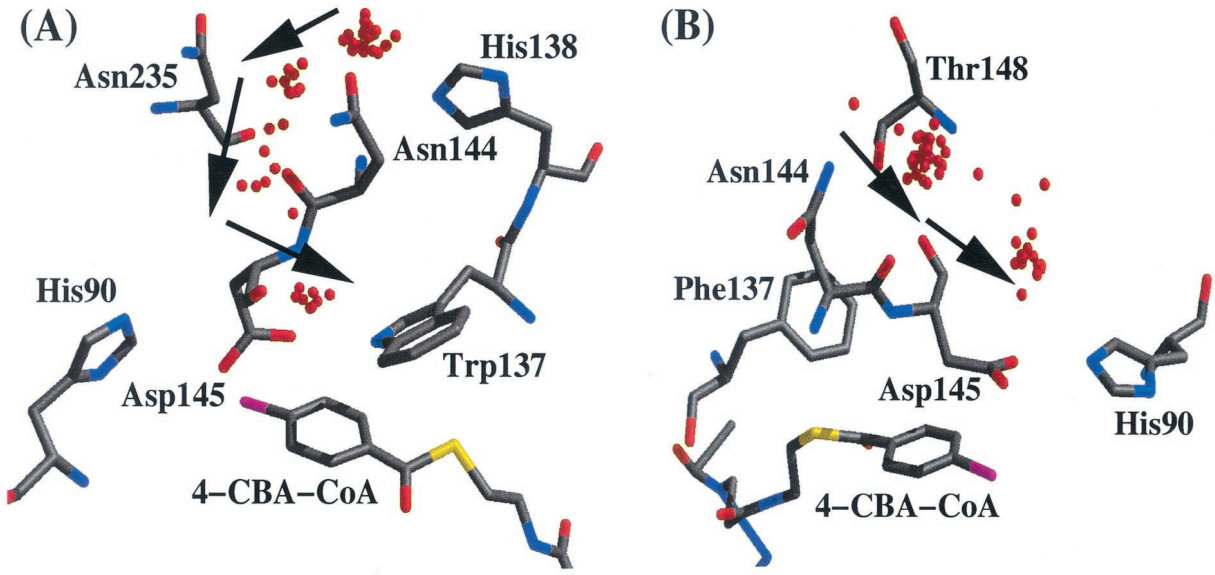

Fig. 6. The paths taken by a single water molecule over time to enter the active sites of the WT (*A*) and W137F (*B*) enzymes. The arrows show the direction the water molecule takes during the trajectory.

at least two conformations exist for the side chain of Asp-145 in the unmodified dehalogenase.

The molecular dynamics simulation of the WT enzyme presents a possible pathway for a water molecule to diffuse into the active site. Initially, a crystallographic water (Xtal75) is hydrogen-bonded to NE2 of His-138 and OD1 of Asn-144 at the beginning of the simulation. This water remains in close contact with the side chains of these residues for the majority of the simulation. After 900 ps of production dynamics, the hydrogen bond between NE2 of His-138 and the water molecule breaks (see Fig. 5*A*). The water molecule enters the active site after ≈1 ns of production dynamics by diffusing between Asn-144 of subunit A and Asn-235 of subunit B (Fig. 6*A*). Once the water molecule enters the active site, it hydrogen-bonds with OD1 of Asp-145. This interaction would not be a favorable one from the standpoint of catalysis because the additional hydrogen bond would decrease the nucleophilicity of the carboxylate, which is already hydrogen-bonded to Trp-137. In addition, the charge on the carboxylate makes it unlikely this hydrogen bond with the water molecule will be broken easily. Probably, it is not favorable for the catalytic water to enter the active site with the charged carboxylate. A more likely scenario would have the water molecule entering the active site after the Meisenheimer intermediate is formed. The charge distribution of the carboxylate is more diffuse in the Meisenheimer intermediate. The carboxylate has changed almost to an ester for this complex. The water also could enter into the active site after formation of the ester intermediate if the chloride is not in the water molecule's path. The charge distribution of the reactants in either case is less than in the Michaelis complex, which would allow greater mobility for the water molecule, thereby allowing it to find the optimal position in the active site for the hydrolysis reaction.

A crystallographic water molecule also was able to diffuse into the active site in the W137F simulation. The water molecule (Xtal31) initially was hydrogen-bonded to ND2 of Asn-144. After 5 ps of production dynamics, the water molecule diffused away from Asn-144 to interact with the backbone amide N and the OG1 of Thr-148. This interaction was stable for ≈150 ps; after this time, the water molecule entered the active site and hydrogen-bonded with NE2 of His-90 and OD2 of Asp-145 for the remainder of the simulation (Fig. 6*B*). Although the conformation between His-90 and Asp-145 in this simulation will not lead to catalysis, it is interesting that a water molecule is able to diffuse into the active site and is positioned between these two catalytic residues.

Conclusions

From the molecular dynamics simulation of WT 4-CBA-CoA dehalogenase, it was found that almost 5% of the active-site conformations formed between Asp-145 and 4-CBA-CoA are NACs. Only the carboxylate oxygen of Asp-145 hydrogen-bonded to Trp-137 was in position to react with the BC4 of 4-CBA-CoA. In the W137F mutant simulation, the hydrogen bond between the catalytic residues His-90 and Asp-145 was stable throughout the trajectory and prevented Asp-145 from making a NAC. Both simulations were able to show that a water molecule is able to diffuse into the active site of 4-CBA-CoA dehalogenase. In the case of the W137F simulation, the water molecule not only entered the active site of 4-CBA-CoA dehalogenase, but also ended up positioned between the catalytic residues His-90 and Asp-145.

We thank Prof. Debra Dunaway-Mariano for bringing the W137F dehalogenase to our attention and Prof. Hazel Holden for providing the W137F dehalogenase crystal structure. We gratefully acknowledge computer time on the Origin2000 supercomputer of University of California, Santa Barbara, which is partially funded by grants from the National Science Foundation and Silicon Graphics, Inc. This study was funded by National Science Foundation Grant MCB-9727937.

1. Yang, G., Liang, P.-H. & Dunaway-Mariano, D. (1994) *Biochemistry* **33,** 8527–8531.
2. Crooks, G. P., Xu, L., Barkley, R. M. & Copley, S. D. (1995) *J. Am. Chem. Soc.* **117,** 10791–10798.
3. Nardi-Dei, V., Kurihara, T., Park, C., Miyagi, M., Tsunasawa, S., Soda, K. & Esaki, N. (1999) *J. Biol. Chem.* **274,** 20977–20981.
4. Stucki, G. & Thuer, M. (1994) *Appl. Microbiol. Biotechnol.* **42,** 167–172.
5. Elsner, A., Loffler, F., Miyashita, K., Muller, R. & Lingens, F. (1991) *Appl. Environ. Microbiol.* **57,** 324–326.
6. Savard, P., Charest, H., Sylestre, M., Shareck, F., Scholten, J. D. & Dunaway-Mariano, D. (1992) *Can. J. Microbiol.* **38,** 1074–1083.

7. Chang, K.-H., Liang, P.-H., Beck, W., Scholten, J. D. & Dunaway-Mariano, D. (1992) *Biochemistry* **31,** 5605–5610.
8. Benning, M. M., Taylor, K. L., Liu, R.-Q., Yang, G., Xiang, H., Wesenberg, G., Dunaway-Mariano, D. & Holden, H. M. (1996) *Biochemistry* **35,** 8103–8109.
9. Liu, R.-Q., Liang, P.-H., Scholten, J. & Dunaway-Mariano, D. (1995) *J. Am. Chem. Soc.* **117,** 5003–5004.
10. Yang, G., Liu, R.-Q., Taylor, K. L., Xiang, H., Price, J. & Dunaway-Mariano, D. (1996) *Biochemistry* **35,** 10879–10885.
11. Taylor, K. L., Liu, R.-G., Liang, P.-H., Price, Z. J., Dunaway-Mariano, D., Tonge, P. J., Clarkson, J. & Carey, P. R. (1995) *Biochemistry* **34,** 13881–13888.
12. Clarkson, J., Tonge, P. J., Taylor, K. L., Dunaway-Mariano, D. & Carey, P. R. (1997) *Biochemistry* **36,** 10192–10199.
13. Taylor, K. L., Xiang, H., Liu, R.-Q., Yang, G. & Dunaway-Mariano, D. (1997) *Biochemistry* **36,** 1349–1361.
14. Brooks, C. L., III, & Karplus, M. (1989) *J. Mol. Biol.* **208,** 159–181.
15. Brooks, B. R., Bruccoleri, R. E., Olafson, B. D., States, D. J., Swaminathan, S. & Karplus, M. (1983) *J. Comput. Chem.* **4,** 187–217.
16. Jorgensen, W. L., Chandrasekhar, J., Madura, J. D., Impey, R. W. & Klein, M. L. (1983) *J. Chem. Phys.* **79,** 926–935.
17. Breneman, C. M. & Wiberg, K. B. (1990) *J. Comput. Chem.* **11,** 361–373.
18. Frisch, M. J., Trucks, G. W., Schlegel, H. B., Scuseria, G. E., Robb, M. A., Cheeseman, J. R., Zakrzewski, V. G., Montgomery, J. A., Stratmann, R. E., Burant, J. C., *et al*. (1998) GAUSSIAN 98 (Gaussian, Carnegie, PA), Version A.6.
19. Brünger, A. T., Brooks, C. L., III, & Karplus, M. (1985) *Proc. Natl. Acad. Sci. USA* **82,** 8458–8462.
20. Brooks, C. L., III, Karplus, M. & Pettitt, B. M. (1987) *Proteins: A Theoretical Perspective of Dynamics, Structure, and Thermodynamics* (Wiley, New York).
21. Ryckaert, J. P., Ciccotti, G. & Berendsen, H. J. C. (1977) *J. Comput. Phys.* **23,** 327–341.
22. Dong, J., Xiang, H., Luo, L., Dunaway-Mariano, D. & Carey, P. R. (1999) *Biochemistry* **38,** 4198–4206.
23. Zheng, Y.-J. & Bruice, T. C. (1997) *J. Am. Chem. Soc.* **119,** 3868–3877.
24. Bruice, T. C. & Lightstone, F. C. (1999) *Acc. Chem. Res.* **32,** 127–136.
25. Bruice, T. C. & Benkovic, S. J. (2000) *Biochemistry* **39,** 6267–6274.
26. Lightstone, F. C. & Bruice, T. C. (1996) *J. Am. Chem. Soc.* **118,** 2595–2605.